Z. Kristallogr. **218** (2003) 542–552

Wickenburgite, a double-layer silicate $Pb_3Al^{[6]}[Ca^{[6]}Al^{[4]}Si^{[4]}_{10}O_{27}(H_2O)_3] \cdot H_2O$: crystal chemistry and thermal behaviour

K.-F. Hesse, F. Liebau* and H.-H. Eulert

Institut für Geowissenschaften, Abt. Mineralogie/Kristallographie, Christian-Albrechts-Universität, Olshausenstraße 40, D-24098 Kiel, Germany

Dedicated to Stefano Merlino in appreciation of his contributions to the crystal chemistry of silicate minerals

Received June 19, 2002; accepted February 20, 2003

Abstract. To clarify discrepancies in the literature with regard to the water content and crystal structure of wickenburgite, chemical and thermal analyses and IR spectroscopic measurements were made and the structure was redetermined with single-crystal X-ray diffraction data. It was found that the idealised composition of the mineral is $Pb_3Al_2CaSi_{10}O_{27} \cdot 4\,H_2O$ rather than $Pb_3Al_2CaSi_{10}O_{27} \cdot 3\,H_2O$ as reported by Lam et al. in 1994. Based on chemical analysis and crystal structure determination, there is considerable isomorphous replacement on the cation positions, leading to the crystal-chemical formula

$$Pb_3(Al_{0.79}Pb_{0.22})^{[6]}_{\Sigma 1.01}\{\boldsymbol{uB}, 4, 2^2_\infty\}$$
$$[Ca^{[6]}_{1.02}(Al_{0.81}Fe_{0.06}Si_{0.14})^{[4]}_{\Sigma 1.01}Si^{[4]}_{10.00}O_{27}(H_2O)_3] \cdot H_2O\,.$$

With regard to crystal structure, that described by Lam et al. is found to be essentially correct, except for an additional H_2O molecule per formula unit, whereas the structure suggested by Penna & Giese in 1968 and by Hesse & Liebau in 1992 and 1993 is incorrect.

The wickenburgite structure contains silicate double-layers in which one out of twelve $[(Al, Si)O_4]$ tetrahedra is replaced by an $[O_3Ca(H_2O)_3]$ octahedron. Adjacent double layers are held together by Al^{3+} and Pb^{2+} cations that are octahedrally and irregularly eight-fold coordinated, respectively. The fourth H_2O molecule per formula unit occupies a small cavity which is formed by six oxygen atoms from two adjacent double layers and three interlayer lead ions, thus shielding the repulsive forces between the lone-pair electrons of the latter.

Minor but varying amounts of adhering, non-crystalline water is reversibly lost upon heating below 100 °C. The cavity water is steadily and irreversibly lost between approximately 100 and 550 °C (at a heating rate of 10 °C per minute). Before all cavity water has been driven out, water coordinating the Ca^{2+} ions begins to escape. This dehydration process is accompanied by an approximately 4.4 percent reduction of the unit-cell volume without substantial disruption of the structure. At 740 °C the dehydration is not yet complete.

The structure of wickenburgite is related to that of jagoite which contains both silicate single- and double-layers. In the double-layers of wickenburgite one out of twelve $[(Al, Si)O_4]$ tetrahedra is replaced by an $[O_3Ca(H_2O)_3]$ octahedron whereas in jagoite within the double-layers two out of twelve $[(Fe, Si)O_4]$ tetrahedra are replaced by $[PbO_3]$ pyramids.

1. Introduction

Wickenburgite is a hydrous lead calcium aluminium silicate which has so far only been described from various localities near Wickenburg, Maricopa County, Arizona, USA (Williams, 1968; Hesse, Liebau, 1992, 1993; Lam, Groat, Cooper, Hawthorne, 1994). While Williams gave a detailed petrological description, Penna and Giese (1968) and Hesse and Liebau reported only short abstracts of crystal structure determinations, whereas Lam et al. described detailed results of a full structure analysis. The main results of these studies are given in Table 1. It can be seen that the various groups derived the same unit cell size, but different chemical compositions, space-group symmetries and crystal structures. To clarify these disagreements and, in particular, to decide whether the crystals studied by Penna and Giese and by Hesse and Liebau, on the one hand, and the ones studied by Lam et al. on the other, represent two different minerals or just one, the present investigation was undertaken.

2. Experimental procedures

2.1 Sample description

The material used in this study was from the same sample as that used in the earlier studies by Hesse and Liebau (1992, 1993). It came from Rat Tail Claim near Wickenburg, Maricopa County, Arizona, USA. In agreement with the first description by Williams (1968) of wickenburgite from the Potter-Cramer Mine near Wickenburg, our crystals were platy and usually formed subparallel, twisted ag-

---

* Correspondence author (e-mail: liebau@min.uni-kiel.de)

Table 1. Chemical composition, unit-cell size, space-group symmetries, and crystal-chemical formulas reported for wickenburgite and, for comparison, of jagoite.

Authors (year)	PbO : CaO : Al_2O_3 : SiO_2 : H_2O (analysis method)	Unit-cell size a [Å], c [Å]	Space group (nr.)	Crystal-chemical formula
Wickenburgite				
Williams (1968)	3 : 1 : 1 : 10 : 3 (chemical anal.)	8.53(1), 20.16(2)	$P6_3/mmc$ *(194)*	–
Penna, Giese (1968)	3 : 1 : 1 : 10 : 3 (crystal struct. anal.)	8.541, 20.181	$P\bar{6}2c$ *(190)*	$Pb_3Ca[Al_2Si_{10}O_{24}(OH)_6]$
Hesse, Liebau (1992, 1993)	3 : 1 : 1 : 10 : 4 (EMA, DTA, TGA, crystal struct. anal.)	8.569(1), 20.216(2)	$P\bar{6}2c$ *(190)*	$H_2Pb_3Ca[Al_2Si_{10}O_{28}] \cdot 3\ H_2O$
Lam et al. (1994)	3 : 1 : 1 : 10 : 3 (crystal struct. anal.)	8.560(3), 20.190(6)	$P31c$ *(159)*	$Pb_3Al[Ca^{[6]}AlSi_{10}O_{27}] \cdot 3\ H_2O$
Present investigation	3 : 1 : 1 : 10 : 4 (EMA, DTA, DSC, TGA, crystal struct. anal.)	8.555(2), 20.190(5)	$P31c$ *(159)*	$Pb_3Al^{[6]}[Ca^{[6]}AlSi_{10}O_{27}$ $(H_2O)_3] \cdot H_2O$
Jagoite				
Mellini, Merlino (1981)	–	8.528(8), 33.33(3)	$P\bar{6}2c$ *(190)*	$Pb_6Fe_2[Pb_2^{[3]}(Si, Fe)_{10}O_{27}]$ $[Fe^{[6]}(Si, Fe)_5O_{17}]Cl_3$

gregates. Under the polarising microscope only few crystals were homogeneous enough to be considered as single crystals. One of them, however, turned out, after back-scattered electron study, to be an oriented intergrowth of two phases: thin darker laths (phase X) within a lighter matrix of wickenburgite. The lath axes formed 60 ° angles with another. In each of the two phases the intensity of the back-scattered electrons was very uniform, suggesting that each phase is of rather homogeneous chemical composition.

2.2 Chemical, thermal and spectroscopic analyses

Electron microprobe analyses (EMA) of two wickenburgite crystals and one crystal of wickenburgite with intergrown laths of phase X were performed on a CAMEBAX Microbeam run at 15 kV and 15 nA, using the correction program of Pouchou and Pichoir (1984). Standards used were wollastonite for Si and Ca, periclase (Philips) for Mg, corundum (Philips) for Al, narsarsukite for Na, silicate glass (NBS) for K, and PbS and lead silicate for Pb. Results of the EMA are presented in Table 2.

Table 2. Chemical compositions of wickenburgite (W_A to W_C) and phase X (X_C) derived by electron microprobe analyses of three crystals. Cation numbers are scaled to 54 non-water oxygen atoms. Estimated errors in parentheses are based on the variance of the data. Corresponding values derived by Williams (1968) by wet chemical analysis of wickenburgite are given in column W_W for comparison.

Crystal No. of points	W_A 5	W_B 4	W_C 4	Average 13	W_W	X_C 2
Oxides	Weight% of oxides					
PbO	46.5(9)	44.7(2)	46.3(4)	45.8	44.0	51.9(2)
CaO	3.66(12)	3.70(3)	3.71(6)	3.69	3.80	2.70(12)
Al_2O_3	5.7(3)	3.9(2)	6.1(1)	5.22	7.6	6.4(1)
SiO_2	38.2(11)	37.7(3)	41.2(4)	39.0	42.1	36.5(4)
Fe_2O_3	n.d.	0.9(3)	n.d.	0.3		n.d.
Na_2O	0.02(1)	0.01(1)	<0.01	0.01		0.01(1)
K_2O	<0.01	0.04(2)	<0.01	0.01		<0.01
H_2O	4.8[a]	4.8[a]	4.8[a]	4.8[a]	3.77	n.d.
Total	98.9	95.8	102.1	98.9	101.3	97.5
Metals	Number of cations scaled to 54 non-water oxygen atoms					
Pb	6.58(23)	6.55(6)	6.19(6)	6.44	6.02	7.45(5)
Ca	2.06(8)	2.15(4)	1.95(3)	2.05	1.92	1.54(4)
Al	3.51(2)	2.52(11)	3.52(8)	3.18	4.23	4.05(1)
Si	20.04(16)	20.55(5)	20.29(5)	20.29	19.86	19.47(1)
Fe	n.d.	0.39(13)	n.d.	0.13		n.d.
Na	0.02(1)	0.02(1)	<0.01(1)	0.02		0.01(1)
K	<0.01	0.02(1)	0.01(2)	0.01		<0.01
$\sum$ Cat	32.21	32.20	31.96	32.12	32.03	32.52

a: These values correspond to the theoretical water content of 8 H_2O per unit cell.

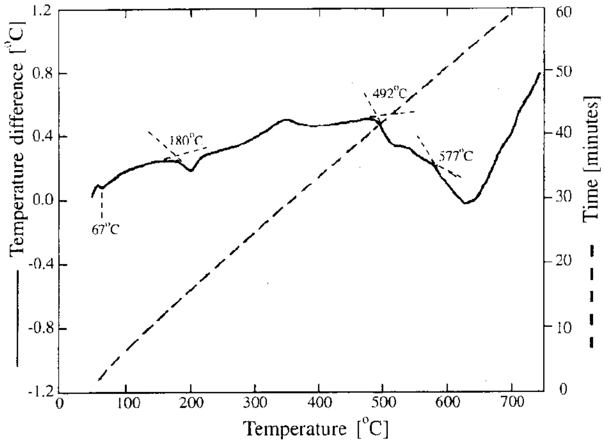

Fig. 1. DTA plot of wickenburgite. Sample size 20.0 mg, heating rate 10 °C per minute.

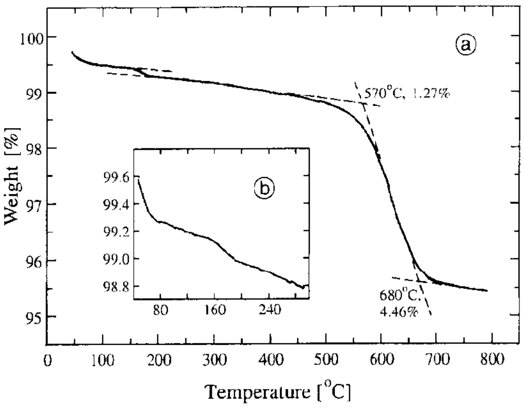

Fig. 3. TGA plots of wickenburgite. (**a**) Sample size 22.76 mg, heating rate 10 °C per minute, (**b**) sample size 14.07 mg, heating rate 10 °C per minute.

Differential thermal analyses (DTA), differential scanning calorimetric analyses (DSC), and thermal gravimetric analyses (TGA) have been performed with a DuPont 1090 Thermal Analyzer System. In most DTA and TGA runs samples of 20 to 25 mg were used. For DSC analyses samples weighted between 3 and 10 mg. The usual heating rate was 10 °C per minute. Representative plots are shown in Figs. 1, 2 and 3, respectively. Their results are summarised in Table 3. In a few cases, the samples were heated with 5 °C per minute, the heating process was interrupted and the sample cooled to room temperature and reheated, or the sample was kept at 480 °C and 740 °C for several hours.

Powder IR spectra have been recorded at room temperature from three samples using the KBr method: (a) original untreated wickenburgite, (b) wickenburgite heated with 10 °C per minute to 230 °C and then cooled to room temperature within 40 minutes, and (c) wickenburgite heated in a DSC run up to 580 °C and cooled to 150 °C with heating and cooling rates of 10 °C per minute. A Bruker IFS 66V Fourier transform spectrometer, operated at a resolution of 2 cm^{-1}, was used to obtain absorption spectra in the range 400 to 4100 cm^{-1}. 96 scans were collected for each spectrum. In Fig. 4 the 2000 to 4100 cm^{-1} regions of the three spectra are compared.

Table 3. Weight loss in percent during TGA and endothermal effects during DTA and DSC heating runs (10 °C per minute) of wickenburgite.

Run	Temp. [°C]											
	67	100	160	180	193	200	450	492	570	577	680	800
TGA 1	0.42	0.53	0.65			0.77	1.12		1.27		4.46	4.60
TGA 2	0.70	0.78	0.90			1.05	1.49		1.68		4.89	
DTA				endo				endo		endo		
DSC	endo				endo							

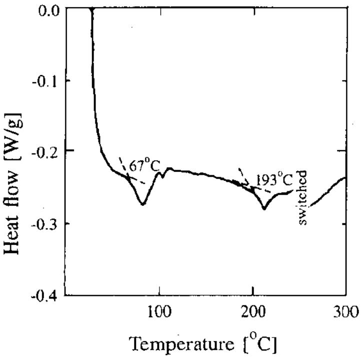

Fig. 2. DSC plot of wickenburgite. Sample size 3.06 mg, heating rate 10 °C per minute. The effect near 220 °C has been shown, by runs without sample, to be an apparatus related effect.

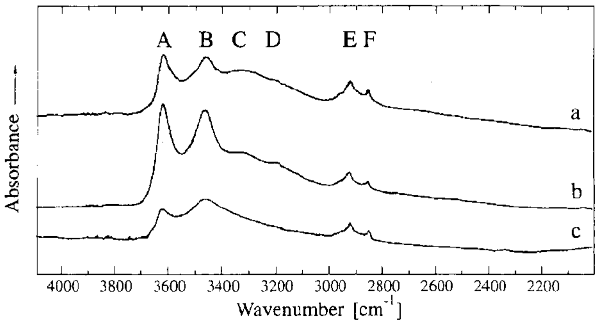

Fig. 4. Powder IR spectra, measured at room temperature, of (**a**) original wickenburgite, (**b**) wickenburgite heated to 230 °C, (**c**) wickenburgite heated to 580 °C.

2.3 Collection of X-ray data, structure redetermination and refinement

Powder diffraction diagrams of heated and unheated wickenburgite (Fig. 5) have been recorded with a SIEMENS D500 Powder Diffractometer, using CuK$_\alpha$ radiation ($\lambda = 1.5406$ Å). Clear wickenburgite crystals were used for X-ray data collection. Details of intensity measurements and refinement of the structure are given in Table 4. The refined unit-cell dimensions, as given in Table 4, were determined with the program DIF4 (Siemens-Software) using 20 reflections measured in the range $15° < 2\theta < 24°$. Lorentz, polarisation and absorption corrections (for empirical absorption corrections the Siemens-Software program EMPIR) were applied to the reflection data. The start positions of the atoms for the refinements were determined using the direct-methods program SHELXS-86 (Sheldrick, 1986). For the cations anisotropic and for the oxygen atoms isotropic atomic displacement parameters were used. Refinement was carried out by full-matrix least-squares methods using the program SHELXL-93 (Sheldrick,

Table 4. Experimental details of the X-ray data collection and structure refinement.

Unit-cell data	
a [Å]	8.555(2)
c [Å]	20.190(5)
V [Å^3]	1279.7(5)
Space group (nr.)	$P31c$ (*159*)
Unit-cell content[a]	2 $Pb_3CaAl_2Si_{10}O_{27} \cdot 4\,H_2O$
Density $D_{calc.}$ [g · cm^{-3}]	3.87
Absorption coefficient μ [mm^{-1}]	20.24
Intensity measurements	
Temperature [°C]	20
Crystal shape	Plate
Crystal size [mm^3]	0.133 × 0.158 × 0.057
Diffraktometer	Siemens-Stoe
Monochromator	Graphite
X-ray radiation (wave length [Å])	MoK_α (0.71069)
2θ range [°]	4.04–60.14
Reflection range	$-12 \le h \le 12$; $-12 \le k \le 12$; $0 \le l \le 28$
Measured reflections	7639
Unique reflections, R_{int}	1287, 0.16(8)
Unique reflections with $F_o > 4\sigma(F_o)$	1019
Structure refinement	
Refinement program	SHELXL-93
Number of refined parameters	92
$R1$ ($F_o > 4\sigma(F_o)$), $R1$ (all reflections)[b]	0.054, 0.071
$wR2$ (all reflections)[c]	0.095
Weight parameters a, b[d]	0.0426, 1.28
Goodness of fit	1.024
Flack parameter	0.008(24)
Extinction coefficient	0.00021(9)
Final $\Delta\varrho_{max}$ [e/Å^3]	2.62
Final $\Delta\varrho_{min}$ [e/Å^3]	−1.39

a: idealized formula

b: $R1 = \sum ||F_o| - |F_c|| / \sum |F_o|$

c: $wR2 = [\sum (w(F_o^2 - F_c^2)^2) / \sum (w(F_o^2)^2)]^{1/2}$

d: $w = 1/[(\sigma(F_o^2))^2 + (aP)^2 + bP]$ with $P = (\max(F_o^2) + 2F_c^2)/3$

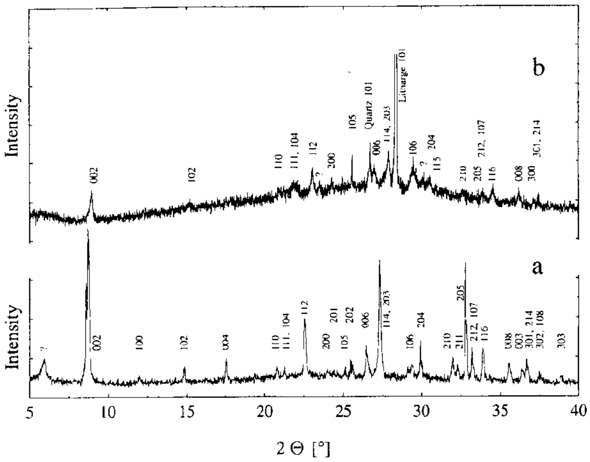

Fig. 5. Indexed X-ray powder diffraction patterns ($\lambda = 1.5406$ Å), taken at room temperature, of (**a**) untreated wickenburgite, (**b**) wickenburgite dehydrated at 740 °C.
"?" not identified.

Table 5. Wyckoff positions, final atomic coordinates and equivalent displacement parameters of wickenburgite.
$U_{eq} = \frac{1}{3} \sum_i \sum_j U_{ij} a_i^* a_j^* \mathbf{a}_i \cdot \mathbf{a}_j$

Atom	Wyckoff position	x	y	z	U_{eq}/U_{iso}
Pb	6*c*	0.2924(1)	0.2593(1)	0.0000[a]	0.0210(2)
Ca	2*a*	0.0000	0.0000	0.1469(5)	0.018(2)
Al	2*b*	0.6667	0.3333	0.4857(6)	0.012(3)
T(1)	2*b*	0.6667	0.3333	0.1283(10)	0.022(4)
T(2)	2*a*	0.0000	0.0000	0.3753(6)	0.016(3)
T(3)	2*b*	0.6667	0.3333	0.2867(6)	0.017(3)
T(4)	2*b*	0.3333	0.6667	0.1972(6)	0.014(3)
T(5)	6*c*	0.384(1)	0.059(1)	0.3751(5)	0.019(2)
T(6)	6*c*	0.060(1)	0.414(1)	0.0962(4)	0.019(2)
T(7)	2*b*	0.3333	0.6667	0.3630(9)	0.016(3)
O(1)	2*b*	0.3333	0.6667	0.275(2)	0.029(9)
O(2)	2*b*	0.6667	0.3333	0.210(2)	0.030(9)
O(3)	2*a*	0.0000	0.0000	0.456(2)	0.026(7)
O(4)	6*c*	0.151(3)	0.492(3)	0.170(1)	0.022(4)
O(5)	6*c*	0.485(3)	0.161(3)	0.103(1)	0.027(5)
O(6)	6*c*	0.520(3)	0.135(3)	0.313(1)	0.023(4)
O(7)	6*c*	0.130(2)	0.571(2)	0.042(1)	0.029(4)
O(8)	6*c*	0.191(2)	0.032(3)	0.347(1)	0.030(4)
O(9)	6*c*	0.081(2)	0.241(2)	0.077(1)	0.027(4)
OW(10)	6*c*	0.232(2)	0.195(3)	0.220(1)	0.035(5)
O(11)	6*c*	0.447(2)	0.210(2)	0.435(1)	0.019(3)
O(12)	6*c*	0.506(3)	0.637(3)	0.397(1)	0.021(5)
OW(13)	2*b*	0.27[b]	0.64[b]	0.51[b]	0.28

a: The z coordinate of Pb was arbitrarily set to zero during origin fixing.

b: Atomic coordinates of OW(13) obtained from a difference Fourier synthesis have been fixed in the final refinement cycle.

Table 6. Selected interatomic distances [Å] and angles [°] in wickenburgite.

Pb–O(9)		2.34(2)
Pb–O(7)		2.38(2)
Pb–O(11)		2.44(2)
Pb–O(3)		2.53(1)
Pb–OW(13)		2.58(>5)
Pb–OW(13)		2.94(>5)
Pb–O(9)		2.98(2)
Pb–O(5)		3.02(2)
Pb–O(12)		3.22(2)
Pb–O(12)		3.35(2)
Pb–OW(13)		3.38(>6)
Ca–O(9)	3×	2.30(2)
Ca–OW(10)	3×	2.36(2)
average		2.33
$Al^{[6]}$–O(7)	3×	1.89(2)
$Al^{[6]}$–O(11)	3×	1.93(2)
average		1.91
T(1)–O(5)	3×	1.60(2)
T(1)–O(2)		1.65(5)
average		1.61
T(2)–O(8)	3×	1.63(2)
T(2)–O(3)		1.63(4)
average		1.63
T(3)–O(2)		1.55(5)
T(3)–O(6)	3×	1.62(2)
average		1.60
T(4)–O(1)		1.57(4)
T(4)–O(4)	3×	1.63(2)
average		1.61
T(5)–O(6)		1.61(2)
T(5)–O(12)		1.61(2)
T(5)–O(11)		1.64(2)
T(5)–O(8)		1.65(2)
average		1.63
T(6)–O(7)		1.60(2)
T(6)–O(9)		1.62(2)
T(6)–O(5)		1.65(2)
T(6)–O(4)		1.66(2)
average		1.63
T(7)–O(12)	3×	1.76(2)
T(7)–O(1)		1.78(5)
average		1.77
OW(10)···O(8)		2.85(2)
OW(10)···O(4)		3.11(3)
OW(10)···OW(10)	2×	3.20(2)
OW(10)···O(9)		3.26(3)
OW(10)···O(2)		3.30(3)
OW(10)···O(5)		3.32(3)
OW(10)···O(8)		3.32(3)
OW(10)···O(6)		3.34(3)
OW(13)···O(5)		2.21^a
OW(13)···O(5)		2.41^a
OW(13)···O(12)		2.58^a
OW(13)···O(5)		2.71^a
OW(13)···O(12)		2.84^a
OW(13)···O(7)		3.03^a
OW(13)···O(12)		3.05^a
T(4)–O(1)–T(7)		180
T(1)–O(2)–T(3)		180
T(4)–O(4)–T(6)		136(1)
T(1)–O(5)–T(6)		151(2)
T(3)–O(6)–T(5)		135(1)
T(2)–O(8)–T(5)		139(1)

a: Due to statistical occupation of the OW(13) position not all of these distances are verified. The standard deviations of these distances are ca. 0.1 Å.

1993). Atomic scattering factors for neutral atoms were taken from the International Tables for X-ray Crystallography Vol. IV (1974) for Pb and Ca, and from SHELXL-93 for Al, Si, and O.

Towards the end of the structure refinement, particular attention has been given to the two H_2O molecules per unit cell that are lost between ca. 100 and 500 °C (see Fig. 3 and section on thermal behaviour of wickenburgite), but had so far not been located. Both visual inspection of the structure and application of the program PLATON (Spek, 1990) revealed two small voids per unit cell around the threefold rotation axes of Wyckoff position 2*b* at $^1/_3$, $^2/_3$, 0.500. A difference Fourier synthesis $\varrho_{obs} - \varrho_{calc}$ ($Pb_3Al_2CaSi_{10}O_{27} \cdot 3\,H_2O$) showed three well resolved maxima at the general position 0.27, 0.64, 0.51, approximately 0.47 Å off the trigonal axis. This indicates that the OW(13) atom of the additional H_2O molecule statistically occupies this position.

Refinement of the structure under the assumption that the crystal used for data collection is a single crystal gave a Flack parameter value of 0.034(38), *R*-values $R1 = 0.082$ and $wR2 = 0.174$, and GOOF = 1.898, indicating that the crystal is twinned. Of the two possibilities, inversion twin and (001) reflection twin with twin matrix

$$\begin{pmatrix} 1 & 0 & 0 \\ 0 & 1 & 0 \\ 0 & 0 & \bar{1} \end{pmatrix},$$

the latter refinement lead to 0.008 (24) for the Flack parameter, $R1 = 0.054$, $wR2 = 0.095$ and GOOF = 1.024 for the larger of the two twin fractions of 70.8(7) and 29.2(7)%. Final atomic parameters given in Table 5 refer to the major twin fraction. Final values of anisotropic atomic displacement factors of the cations have been deposited[1]. Values

---

[1] Additional material to this paper, such as anisotropic atomic displacement factors of the cations can be ordered referring to the CSD number 413021, names of the authors and citation of the paper at the Fachinformationszentrum Karlsruhe, Gesellschaft für wissenschaftlich-technische Information mbH, D-76344 Eggenstein-Leopoldhafen, Germany. The list of F_o/F_c-data is available from the author up to one year after the publication has appeared.

Table 7. Calculated bond valences and bond-valence sums [v.u.] for wickenburgite.

Cat. Ox.	Pb	Ca	$Al^{[6]}$	T(1)	T(2)	T(3)	T(4)	T(5)	T(6)	T(7)	$\sum s(Ox)$
O(1)							1.17			0.70	1.87
O(2)				0.94		1.22					2.16
O(3)	0.32 (3x →)				0.98						1.94
O(4)							1.00 (3x ↓)		0.91		1.90
O(5)	0.09			1.06 (3x ↓)					0.93		2.08
O(6)						1.03 (3x ↓)		1.04			2.07
O(7)	0.48		0.52 (3x ↓)						1.08		2.08
O(8)					1.00 (3x ↓)			0.93			1.93
O(9)	0.54, 0.10	0.41 (3x ↓)							1.02		2.07
OW(10)		0.34 (3x ↓)									0.34
O(11)	0.41		0.47 (3x ↓)					0.95			1.83
O(12)	0.05, 0.04							1.0 4		0.74 (3x ↓)	1.86
OW(13)	0.29, 0.11, 0.03 (1/3 each)			0.11							0.25
$\sum s(Cat)$	2.17	2.25	2.96	4.24	3.97	4.29	4.15	3.96	3.93	2.92	

of selected bond lengths and TOT angles are listed in Table 6. Bond valences and bond-valence sums have been calculated using the bond-valence parameters tabulated by Brese and O'Keeffe (1991) and are given in Table 7.

3. Results and discussion

3.1 Wickenburgite

3.1.1 Crystal structure

The crystal structure determined in this study and shown in Figs. 6 and 7 is very similar to that described by Lam et al. (1994). Therefore, instead of a detailed description only those aspects of the structure are treated which have not been discussed by Lam et al.

Silicate anions

Following the silicate classification of Liebau (1985), the IUCr recommendation on nomenclature by Lima-de-Faria, Hellner, Liebau, Makovicky and Parthé (1990), and the recommendation on structure-type formulas by Smith, Roberts, Bayliss and Liebau (1998), in wickenburgite [TO_4] tetrahedra with **T** = Si, Al, Fe share corners to form a trigonal unbranched *vierer* single layer described by

$$\{uB, 4, 1^2_\infty\}\ [(\mathbf{T}(2)\,\mathbf{T}(3)\,\mathbf{T}(5)_3\,\mathbf{T}(7))^{[4t]}O_{15}]\ \text{(sublayer 1)}$$

(Fig. 6). Here the information within the curly brackets are the branchedness (***uB***) and the periodicity ($P^C = 4$) of the fundamental chain, the multiplicity ($M = 1$) and the dimensionality ($D = 2$) of sublayer 1. The tetrahedrally coordinated cations **T**(3) and **T**(7) share one oxygen atom each (O(2) and O(1)) with tetrahedrally coordinated cations **T**(1) and **T**(4), respectively, of another sublayer. This second sublayer is also a trigonal unbranched *vierer*

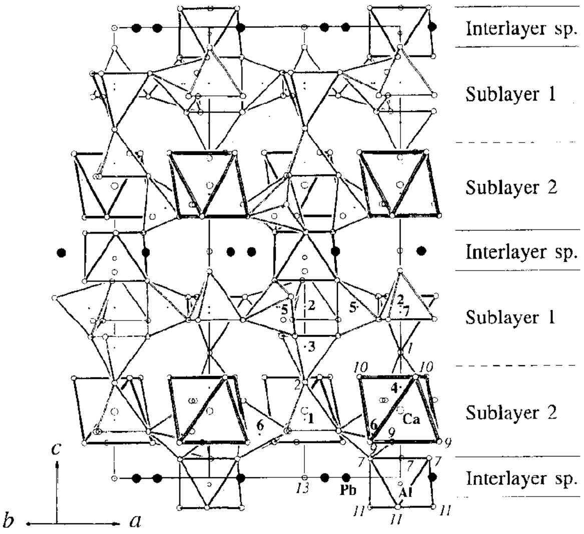

Fig. 6. Crystal structure of wickenburgite projected onto (010). Bold-type numbers refer to **T** atoms, non-bold italic numbers to oxygen atoms.

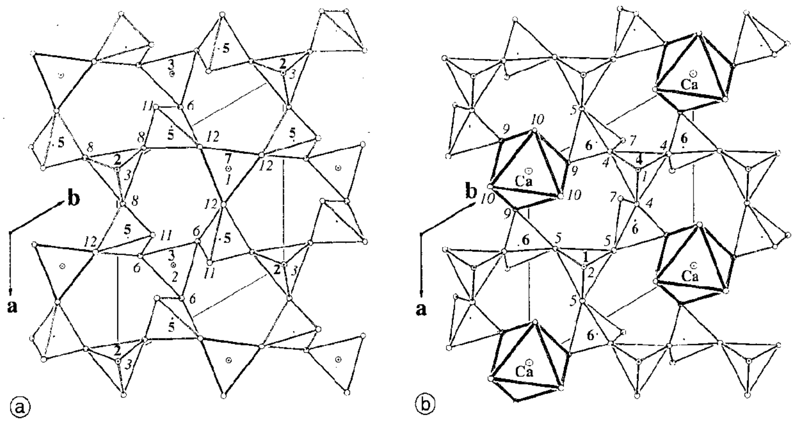

Fig. 7. Projection of the sublayers of wickenburgite onto (001). (**a**) Sublayer 1, (**b**) sublayer 2. Bold-type numbers refer to **T** atoms.

single layer in which, however, one tetrahedron is replaced by an $[O_3Ca(H_2O)_3]$ octahedron:

$\{\boldsymbol{uB}, 4, 1^2_\infty\}$ $[Ca^{[6o]}(\mathbf{T}(1)\,\mathbf{T}(4)\,\mathbf{T}(6)_3)^{[4t]}O_{14}(H_2O)_3]$ (sublayer 2).

That the OW(10), coordinating the calcium ions, represent water oxygen atoms is in agreement with their low bond-valence sums of 0.34 v.u. (Table 7).

The crystal chemical formula of the double layer can be written as

$\{uB, 4, 2^2_\infty\}$ $[Ca^{[6o]}T^{[4t]}_{11}O_{27}(H_2O)_3]$,

where the three H_2O molecules of the octahedron can be considered as intralayer species. Unfortunately, the accuracy of the wickenburgite structure derived by Lam et al. (1994), as well as that presented here, is only fair. This is apparently due to the poor quality of the crystals which showed parallel (twinning) and subparallel intergrowth, and sometimes, in addition, oriented intergrowth with a second phase that is richer in Pb and Al (phase X in Table 2). Therefore, bond lengths and bond angles listed in Table 6 are not discussed in detail. It should, however, be noted that the calculated angles of the **T**(1)O(2)**T**(3) and **T**(7)O(1)**T**(4) bonds linking the two sublayers are 180°, because all these atoms have been located on trigonal rotation axes.

Interlayer species

Adjacent silicate double layers are held together by lead atoms in irregular coordination and by, mainly, aluminium atoms in almost regular octahedral coordination with oxygen atoms of adjacent double layers. For the moment not taking into account the water oxygen atom OW(13), each eight-coordinated lead atom has four short bonds (2.34–2.53 Å) on one side and four longer ones (2.98–3.35 Å) on the other (Table 6, solid and thick open lines respectively in Fig. 8). This aspheric coordination reflects the stereoactive influence of the lone-electron pair (LEP) of the lead atoms on the geometry of the $[PbO_n]$ polyhedron. The electron density of the LEP of a lead atom is concentrated at the side with the longest Pb–O distances, such that the LEPs of each triple of lead atoms are directed approximately towards the Wyckoff positions 2*b* on the threefold rotation axes. Consequently, the LEPs of the three lead atoms shown in Fig. 8 repel another, thus creating the void around the special position $^1/_3$, $^2/_3$, 0.500. This void is statistically occupied by the OW(13) atoms in a general position 0.47 Å off the 3-fold rotation axis. The bond-valence sum of 0.25 v.u. (Table 7) indicates that OW(13) represents a H_2O molecule. The coordination of each Pb atom is then supplemented by OW(13) atoms at distances of 2.58, 2.94 and 3.38 Å, each one with a 33 percent occupancy. The $H_2O(13)$ molecules fulfil two purposes: (i) they shield the Pb^{2+} from repulsion between their LEPs and (ii) they fill the void space thus adding to the lattice energy by forming weak bonds to Pb^{2+} and, perhaps, hydrogen bonds to O(12) (bond-valence sum s = 1.86 v.u.).

Cation distribution

Information on the distribution of the cations over the various structure sites can be drawn from the chemical analyses of the three crystals W_A, W_B and W_C (Table 2), and from least squares refinements with unrestrained site occu-

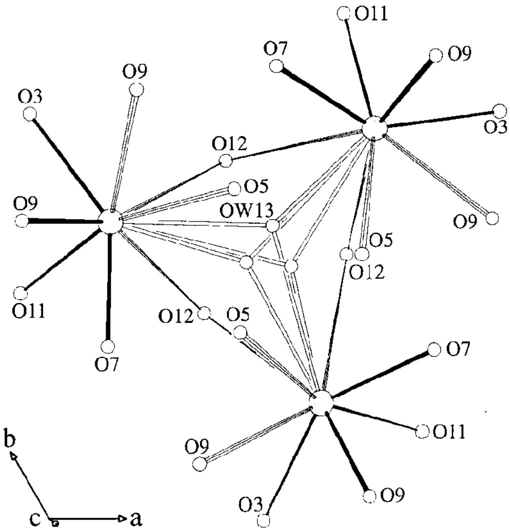

Fig. 8. Schematic representation of $[PbO_n]$ polyhedra around the intralayer water oxygen-atoms OW(13) which statistically occupy the split positions around $^1/_3$, $^2/_3$, 0.500 of wickenburgite. Solid lines: short PbO bonds to oxygen atoms of the silicate layer; bonds shown as triple lines: long PbO bonds to oxygen atoms of the silicate layers; open lines: PbO bonds to oxygen atoms OW(13) of the statistically distributed H_2O molecule.

pation factors and bond-valence calculations (Table 7) derived for a fourth crystal.

Although the particular cation numbers per formula unit of wickenburgite derived from EMA show considerable variation from crystal to crystal and although in particular the numbers of lead and aluminium atoms deviate considerably from integers (Table 2), for each analysed crystal the sum of all cations per crystallographic unit cell is near to 32, which is the number of cation positions per unit cell derived in the crystal structure refinement. This suggests that the differences in the compositions of the wickenburgite crystals is essentially caused by differences in mutual cation replacement.

Taking into consideration the so-called structure-site formula (Smith, Roberts, Bayliss, Liebau, 1998) for wickenburgite

$$\mathbf{L}_6\mathbf{G}_2^{[6]}[\mathbf{G}_2'^{[6]}\mathbf{T}(1-6)_{20}^{[4]}\mathbf{T}(7)\mathrm{O}_{54}(\mathrm{H_2O})_6]\cdot 2\,\mathrm{H_2O}$$

derived from the structure refinement, it becomes evident, that, in each of the three crystals analysed in Table 2, the excess of aluminium atoms over the 22 (Al, Si and Fe) atoms required to fill the Wyckoff positions **T**(1) to **T**(7) adds up with the number of lead atoms to approximately eight atoms per unit cell. This suggests that the structure-site designated **L** is fully occupied by six Pb atoms per unit cell and that the structure-site **G** is statistically occupied by the remaining lead atoms and the aluminium atoms not required to fill, together with silicon and iron atoms, the **T** positions of the double layer. In addition, perhaps a small amount of calcium atoms may also be located in site **G**. Neglecting the very small amounts of alkali atoms, this leads to the average formula

$$\mathrm{Pb_6(Al_{1.59}Pb_{0.44})^{[6]}_{\Sigma 2.03}[Ca^{[6]}_{2.05}(Al_{1.62}Fe_{0.13}Si_{20.29})^{[4]}_{\Sigma 22.04}}$$
$$\mathrm{O_{54}(H_2O)_6]\cdot 2\,H_2O}$$

for the unit-cell content and to the simplified ("ideal") formula

$$\mathrm{Pb_3Al^{[6]}[Ca^{[6]}Al^{[4]}Si_{10}O_{27}(H_2O)_3]\cdot H_2O}\,.$$

With regard to the distribution of the Si, and the Al atoms remaining over the tetrahedrally coordinated positions **T**(1) to **T**(7), we assume 1.613 Å to be the average bond length ⟨d(**TO**)⟩ of a pure $[\mathrm{SiO_4}]$ tetrahedron [averaged over 1.614, 1.613, 1.613 Å derived for anorthite, low albite, low microcline, respectively, (Kroll, Ribbe, 1983) and 1.613 Å for bikitaite (Bissert, Liebau, 1986)]. The corresponding value of the average bond length of a pure $[\mathrm{AlO_4}]$ tetrahedron is assumed to be 1.743 Å [averaged over 1.747, 1.742, 1.738 and 1.745 Å, respectively, (Kroll, Ribbe, 1983; Bissert, Liebau, 1986)]. Linear interpolation between these two averages, together with the average **TO** bond lengths derived during structure refinement (Table 6) suggests that, within the error limits of the structure refinement, positions T(1) to T(6) are fully occupied by silicon. T(7) is occupied by aluminium, some ferric iron and probably some silicon. This is in agreement with the value 2.92 v.u. calculated for the bond-valence sum $s_{\mathrm{T-O}}$ of T(7), and with the value of 1.77 Å derived for the average bond length ⟨d[**T**(7)O]⟩. The fact that the refinement of the site occupation factors of **T**(7) and **G** did not reveal an excess of electrons indicates that, in the crystal studied, these sites did not contain remarkable amounts of Fe and Pb respectively. Consequently, the crystal used for structure refinement approximates the "ideal" formula, in contrast to crystal $\mathrm{W_B}$ which contains some Fe in **T**(7) and crystals $\mathrm{W_A}$, $\mathrm{W_B}$ and $\mathrm{W_C}$ that contain varying amounts of Pb in the **G** site.

3.1.3 Thermal behaviour of wickenburgite

The thermal behaviour of wickenburgite is deduced from a combination of DTA, DSC and TGA measurements (Figs. 1, 2, 3) and IR spectra, taken at room temperature, of untreated wickenburgite and wickenburgite heated to 230 °C and 580 °C (Fig. 4). These thermal and spectroscopic experiments indicate that the mineral contains three kinds of water:

(i) adhering, non-structural water which is discernible from the two broad IR bands C and D at approximately 3290 $\mathrm{cm^{-1}}$ and 3185 $\mathrm{cm^{-1}}$ (Fig. 4a, b) and

(ii) two kinds of structural water which both give rise to stronger IR bands A, B, and G at 3625 $\mathrm{cm^{-1}}$, 3460 $\mathrm{cm^{-1}}$ and 1615 $\mathrm{cm^{-1}}$, respectively, the latter of which is not shown in Fig. 4. Bands A and B are assigned to asymmetric and symmetric OH stretching modes ν_3 and ν_1 respectively, whereas band G is considered to be associated with the symmetric $\mathrm{H_2O}$ bending mode ν_2. The relatively sharp IR bands E and F at 2915 $\mathrm{cm^{-1}}$ and 2850 $\mathrm{cm^{-1}}$ are attributed to organic impurities (CH-bands), probably originating from the laboratory air.

TGA curves measured at 10 °C per minute, as the one shown in Fig. 3a, reveal a complex dehydration process. Between room temperature and ca. 65 °C there is a weight loss which varies for different samples between approximately 0.4 and 0.9 weight% (Table 3). This weight loss is accompanied by endothermic DTA (Fig. 1) and DSC (Fig. 2) effects. They are attributed to loss of adhering water which is, at least partially, reversible. This reversibility, which is evident from TGA experiments, is responsible for the weak broad IR bands C and D in the spectra of wickenburgite that has been heated to 230 °C (Fig. 4b).

Between 65 °C and ca. 480 °C there is a slow but steady and irreversible weight loss of an additional ca. 0.8 weight% (at 10°C per minute heating rate), which is attributed to expulsion of the $\mathrm{H_2O(13)}$ molecules. Loss of this interlayer water is accompanied by a decrease of the absorbance of the IR band A (Fig. 4c). Before this process comes to an end, the dehydration rate accelerates, increases greatly between 570 and 680 °C and eventually slows down. At the end of the TGA 1 run (Fig. 3, Table 3) at 800 °C there is still a small weight loss. The weight loss above ca. 500 °C is ascribed to the removal of the $\mathrm{H_2O(10)}$ molecules which coordinate to the $\mathrm{Ca^{2+}}$ cations.

Weight losses observed in the TGA runs 1 and 2 (Table 3) between 65 and 570 °C, i.e. after expulsion of the adhering water, amount to 0.85 and 0.98 percent, respectively. Irreversible weight losses above 570 °C are another 3.33 percent (till ca. 800 °C for run 1) and 3.19 percent (till 680 °C for run 2).

Table 8. The proposed distribution of the cations over the various structure sites of the formula $\mathbf{L}_6\mathbf{G}_2^{[6]}[\mathbf{G}_2'^{[6]}\ \mathbf{T}(7)_2\mathbf{T}(1-6)_{20}O_{54}(H_2O)_6]\cdot 2\,H_2O$, derived from the electron microprobe analyses of the three wickenburgite crystals W_A, W_B and W_C (see Table 2). The numbers of lead atoms in structure site **L** and of silicon atoms in structure sites T(1–6) have arbitrarily been set to 6.00 and 20.00, respectively, so that the analytical errors accumulate in structure sites **G**, **G**′ and **T**(7).

Crystal	L	$G^{[6]}$	$G'^{[6]}$	T(7)	T(1–6)	$\sum$ Cat
W_A	$Pb_{6.00}$	$(Al_{1.51}Pb_{0.58})_{\sum 2.09}$	$Ca_{2.06}$	$(Al_{2.00}Si_{0.04})_{\sum 2.04}$	$Si_{20.00}$	32.19
W_B	$Pb_{6.00}$	$(Al_{1.45}Pb_{0.55})_{\sum 2.00}$	$Ca_{2.15}$	$(Al_{1.07}Si_{0.55}Fe_{0.39})_{\sum 2.01}$	$Si_{20.00}$	32.16
W_C	$Pb_{6.00}$	$(Al_{1.81}Pb_{0.19})_{\sum 2.00}$	$Ca_{1.95}$	$(Al_{1.71}Si_{0.29})_{\sum 2.00}$	$Si_{20.00}$	31.95
Average	$Pb_{6.00}$	$(Al_{1.59}Pb_{0.44})_{\sum 2.03}$	$Ca_{2.05}$	$(Al_{1.60}Si_{0.29}Fe_{0.13})_{\sum 2.02}$	$Si_{20.00}$	32.10

Taking into account that, at a heating rate of 10 °C per minute, neither of the two irreversible dehydration processes has come fully to an end at 570 °C and 680 (800) °C respectively, the weight losses during the two processes are considered to correspond to approximately two $H_2O(13)$ molecules per unit cell for the first and six $H_2O(10)$ molecules per unit cell for the latter process. This corresponds to theoretical values of 1.20 and 3.59 weight%, respectively.

At the lower heating rate of 5°C per minute the weight losses are shifted to slightly lower temperatures without changing the overall picture.

Since the interlayer $H_2O(13)$ molecules are only weakly bonded by their neighbours, one would expect that they would be lost below ca. 120 °C, in analogy to the dehydration behaviour of zeolites. Instead, at a heating rate of 10 °C per minute, it needs more than ca. 570 °C and considerable time before this interlayer water is completely lost. This persistence can be explained by the fact that each of these H_2O molecules is firmly enclathrated by six oxygen atom, O(5) and O(12), three from each of the two neighbouring silicate double-layers (Fig. 8). In fact, the thermal behaviour of this water in wickenburgite is similar to that observed for H_2O molecules enclathrated in beryl $Al_2Be_3[Si_6O_{18}]$ and cordierite $(Mg,Fe)_2[Al_4Si_5O_{18}]$ (Aines, Rossman, 1984) and for guest molecules encaged in clathrasils (e.g. Marler, Dehnbostel, Eulert, Gies, Liebau, 1986).

The fact that the intralayer $H_2O(10)$ molecules, which form one triangular face of the $[O_3Ca(H_2O)_3]$ octahedron, are lost at considerably higher temperatures than the interlayer $H_2O(13)$ molecules can be explained by the fact that loss of $H_2O(10)$ would leave the calcium atoms 'naked' on one side, thus requiring considerable rearrangement of the structure.

A sample that had been heated in a TGA run with 10 °C per minute up to 485 °C and had lost 1.3 percent of its weight, still gave an X-ray powder diagram of wickenburgite. Its diffraction lines were even sharper than those of an unheated sample.

DTA and DSC heating curves indicate two endothermic effects at ca. 70 and 190 °C (Figs. 1, 2). Although TGA heating curves display a slight increase of the dehydration rate near 190 °C (Fig. 3), the very small weight loss of ca. 0.15 percent suggests that at least this effect is not due to an independent dehydration process, but rather to a reversible, probably displacive, phase transition of the wickenburgite polyhedron framework.

3.2 Dehydrated wickenburgite

An X-ray powder pattern ($\lambda = 1.5406$ Å) obtained from a sample that was held for four hours at 740 °C strongly resembled that of an unheated sample with regard to 2θ-values and intensities (Fig. 5). With the exception of four reflections (two stronger ones with 2θ-values of 26.70° and 28.32° and two weak ones with $2\theta = 23.43°$ and 30.10°) all other observed reflections have been indexed with a hexagonal unit cell of $a = 8.39(2)$ Å and $c = 19.81(7)$ Å (Table 9) compared to $a = 8.555(2)$ Å and $c = 20.190(5)$ Å for the original unheated material. Extrapolation versus $\cot\theta \times \cos\theta = 0$ of the d_{100} and d_{001} values derived from the experimental powder data, in order to correct for absorption effects (Peiser, Rooksby, Wilson, 1960), lead to $a_{corr} = 8.43(3)$ Å and $c_{corr} = 19.85(5)$ Å.

Table 9. X-ray diffraction data (CuK_α, $\lambda = 1.5406$ Å) of wickenburgite powder that was held at 740 °C for four hours (see Fig. 5). The calculated 2θ-values were derived with $a_{hex} = 8.39$ Å and $c_{hex} = 19.81$ Å.

2_{obs} [Å]	2_{calc} [Å]	I [cps]	*hkl*
8.97	8.92	8.9	002
15.18	15.11	1.3	102
21.27	21.16	1.7	110
21.97	21.64 21.70	3.7	111 104
23.05	23.01	7.9	112
23.43		*2.4*	*n.i.*
24.20	24.48	2.7	200(?)
3.483	3.481	12.3	105
3.336	3.343	18.3	quartz 101
3.307	3.304	7.1	006
3.197	3.203 3.185	ca. 10	114 203
3.145	3.115	714	litharge 101
3.030	3.008	7.6	106
2.968	–	*2.8*	*n.i.*
2.926	2.931	5.0	204
2.645	2.648 2.639	3.0	212 107
2.594	2.596	4.6	116
2.481	2.478	4.7	008
2.421	2.424	3.5	300
2.400	2.403	3.1	214
1.931	1.933	7.8	224

n.i.: not identified

These values correspond to 1.5 percent reduction of the lattice constants and to 4.4 percent reduction of the unit-cell volume during dehydration. This suggests that even after loss of almost all of the eight H_2O molecules per unit-cell the silicate double-layers are still intact.

The two strong reflections not indexed with the wickenburgite-related cell correspond to the strongest reflections of quartz and litharge (tetragonal PbO), respectively. These may have formed, together with an amorphous phase (see the high background intensity in Fig. 5b) during the beginning thermal decomposition or incongruent melting of the wickenburgite. The two weak unindexed reflections (marked with ? in Fig. 5b) could not be associated with the diffraction diagram of a known substance and may be of similar origin.

3.3 Comparison with jagoite

The crystal structure of wickenburgite shows strong similarities with that of jagoite, which is a lead silicate of very complex chemical composition and crystal structure (Mellini, Merlino, 1981). These similarities are obvious from comparisons of lattice constants, symmetry (Table 1) and, in particular, projections of the two structures.

In jagoite, silicate single-layers $\{\boldsymbol{uB}, 4, 1^2_\infty\}$ $[\mathrm{Fe}^{[6o]}\mathrm{T}_5\mathrm{O}_{17}]$ alternate with double layers $\{\boldsymbol{uB}, 4, 2^2_\infty\}$ $[\mathrm{Pb}_2^{[3n]}\mathrm{T}_{10}\mathrm{O}_{27}]$ (Fig. 9). Sublayer 1 of wickenburgite differs from that of the sublayer of the mirror-symmetrical jagoite double-layer by replacement of the tetrahedron $[\mathrm{T(7)O_4}]$ with T = Al, Si of wickenburgite by the ψ-tetrahedron $[\mathrm{Pb(1)O_3E}]$ of jagoite, where E represents the lone-electron pair of the Pb atom (Figs. 7 and 10). As a consequence of this replacement, the linkage that corresponds to the bridge T(7)O(1)T(4) between the two sublayers of wickenburgite is interrupted in the double layer of jagoite (Figs. 6 and 9). Sublayer 2 of wickenburgite differs from the single layer of jagoite by replacement of the $[\mathrm{O_3Ca(H_2O)_3}]$ octahedra of the former by $[\mathrm{Fe(1)O_6}]$ octahedra in the latter.

In wickenburgite the double layers are interconnected by interlayer $\mathrm{Al}^{3+[6o]}$ and Pb^{2+} ions, whereas in jagoite interconnection between adjacent single and double layers is accomplished by $\mathrm{Fe}^{3+[6o]}$ and lead ions $\mathrm{Pb(2)}^{2+}$. The intralayer distance in wickenburgite is limited by relatively short bridges T(1)O(2)T(3) of 3.20 Å and T(4)O(1)T(7) of 3.35 Å between the two sublayers (Fig. 7). This leaves just enough space to accommodate the intralayer H_2O molecules of the $[\mathrm{O_3Ca(H_2O)_3}]$ octahedra. For comparison, in jagoite the intralayer distance 3.54 Å of the (Si, Fe)(2)O(9)(Si, Fe)(2) linkage is considerably longer, partly due to replacement of silicon by iron and partly due to repulsive forces between the LEPs of opposing Pb(1) atoms. As a consequence, the intralayer space of jagoite is wide enough to accommodate lead cations Pb(3) and chloride anions (Fig. 9).

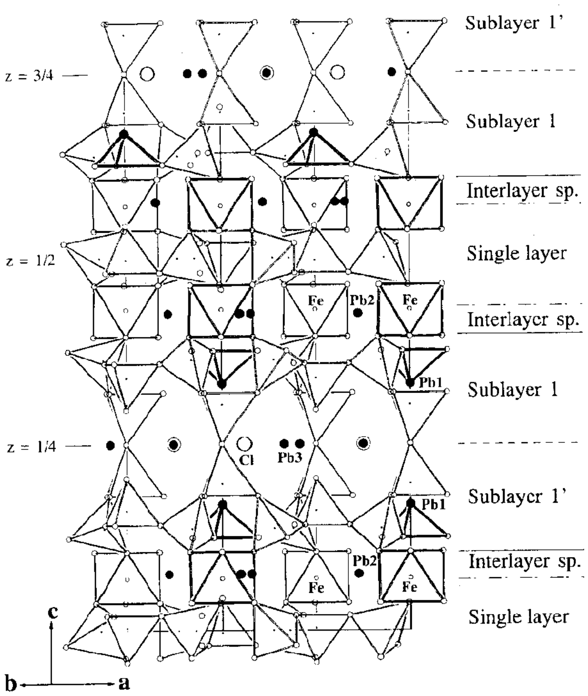

Fig. 9. Crystal structure of jagoite projected nearly along $[00\bar{1}]$. Half of the Fe^{3+} ions of the $[\mathrm{FeO_6}]$ octahedra can either be considered to be part of the $[\mathrm{Fe}^{[6o]}\mathrm{T_5O_{17}}]$ single layer and the other half to belong to the interlayer space, or all the Fe^{3+} can alternatively be considered as interlayer species.

Instead of considering every second $[\mathrm{FeO_6}]$ octahedron as part of the silicate single-layer of jagoite, all the $[\mathrm{FeO_6}]$ octahedra can be regarded alternatively, together with the Pb(2) ions, as interlayer cations between adjacent silicate double- and, incomplete, single-layers.

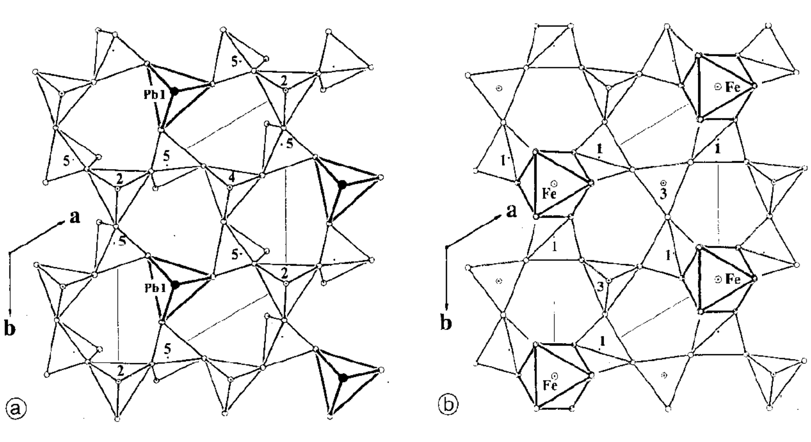

Fig. 10. (a) Projection onto (001) of one sublayer of the mirror-symmetrical double layer of jagoite; (b) projection onto (001) of the single layer of jagoite. Half of the Fe^{3+} ions of the $[\mathrm{FeO_6}]$ octahedra can either be considered to be part of the $[\mathrm{Fe}^{[6o]}\mathrm{T_5O_{17}}]$ single layer and the other half to belong to the interlayer space, or all the Fe^{3+} can alternatively be considered as interlayer species and the single layer as deficient. Bold-type numbers refer to **T** atoms.

3.4 Phase X

Due to the fine lamellar intergrowth between phase X and the wickenburgite matrix, which was observed in one of the crystals, electron microprobe analyses of only two points within one lamella have been measured. The resulting chemical composition given in Table 2 is, therefore, of rather low accuracy. Due to the extensive isomorphous replacement of the cations in wickenburgite as well as in jagoite, no well-founded speculation on the crystal structure of phase X can be made solely based on the chemical composition. Single crystals suitable for structure determination are required to determine the structure of this phase.

4. Conclusions

The present redetermination of the crystal structure of wickenburgite proves that the structure determination by Lam et al. (1994) is largely correct and the one briefly described by both Penna and Giese (1968) and Hesse and Liebau (1992, 1993) is in error. The wrong structure had been derived by us by application of direct methods assuming $P\bar{6}2c$ instead of its subgroup $P31c$ which has the same systematic extinctions as $P\bar{6}2c$. Both structures show considerable resemblances: (i) they contain silicate double layers, (ii) Pb^{2+} ions are located between the silicate double layers and (iii) H_2O molecules occupy the intralayer space. However, although there is a subgroup-supergroup relation between the two space groups, the wrong structure in $P\bar{6}2c$ cannot be derived by distortion of the correct $P31c$ structure. Instead, the two structures have different topologies. The most striking difference between the two structures is that in the correct structure the two sublayers are not symmetrically equivalent. Thus in only one of the two sublayers a $[TO_4]$ tetrahedron is replaced by a $[CaO_6]$ octahedron, whereas the false mirror planes of the $P\bar{6}2c$ structure led to double layers consisting of $[TO_4]$ tetrahedra only. The different topologies of the two structures rule out that there may be a displacive thermal phase transformation of the correct $P31c$ structure into the more symmetrical but wrong $P\bar{6}2c$ structure described by Hesse and Liebau (1992, 1993). Although this does not exclude that a mineral or a synthetic phase with this latter structure can exist, it is unlikely that its trigonal prismatic cation positions are occupied by cations as large and electropositive as Ca^{2+}.

Acknowledgments. We are very grateful to Dr. D. Ackermand for performing the electron microprobe analyses, Dr. P. Schmid-Beurmann and Dipl. min. L. Peters for measuring the IR spectra., Mrs. S. Bass and Dr. H. Katzke for measuring and indexing the X-ray powder diffraction diagrams, and Dr. C. A. Geiger for discussions regarding the interpretation of the IR spectra and critically reading the manuscript. Critical comments by Prof. H. Effenberger and an anonymous reviewer helped to improve the manuscript and are gratefully acknowledged.

References

Aines, R. D.; Rossman, G. R.: The high temperature behavior of water and carbon dioxide in cordierite and beryl. Amer. Mineral. **69** (1984) 319–327.

Bissert, G.; Liebau, F.: The crystal structure of a triclinic bikitaite, $Li[AlSi_2O_6] \cdot H_2O$, with ordered Al/Si distribution. N. Jb. Miner. Mh. (1986) 241–252.

Brese, N. E.; O'Keeffe, M.: Bond-valence parameters for solids. Acta Crystallogr. **B41** (1991) 192–197.

Hesse, K.-F.; Liebau, F.: The crystal structure of wickenburgite, $H_2CaPb_3[Al_2Si_{10}O_{28}] \cdot 3\,H_2O$: another double-layer silicate. Z. Kristallogr. Suppl. **6** (1992) 162.

Hesse, K.-F.; Liebau, F.: Crystal structure and chemical composition of wickenburgite, $H_2Ca^{[6p]}Pb_3{}^{[4n]}$ $\{\boldsymbol{lB}, 2^2_\infty\}$ $[^{[4]}(Al_2Si_{10})O_{28}] \cdot 3\,H_2O$ – the first silicate with loopbranched *vierer* double-layers. Z. Kristallogr. Suppl. **7** (1993) 78.

International Tables for X-ray Crystallography, Vol. IV. Kynoch Press, Birmingham (1974).

Kroll, K.; Ribbe, P. H.: Lattice parameters, composition and Al, Si order in alkali feldspars. Reviews in Mineralogy 2 (2nd ed.) (1983) 57–99.

Lam, A. E.; Groat, L. A.; Cooper, M. A.; Hawthorne, F. C.: The crystal structure of wickenburgite, $Pb_3CaAl[AlSi_{10}O_{27}](H_2O)_3$, a sheet structure. Canad. Mineral. **32** (1994) 525–532.

Liebau, F.: Structural chemistry of silicates. Springer, Berlin, 1985, pp. 52–89; programmed version CRYSTANA: available from http://www.is.informatik.uni-kiel.de/~hjk/crystana.html.

Lima-de-Faria, J.; Hellner, E.; Liebau, F.; Makovicky, E.; Parthé, E.: Nomenclature of inorganic structure types. Acta Crystallogr. **A46** (1990) 1–11.

Marler, B.; Dehnbostel, N.; Eulert, H.-H.; Gies, H.; Liebau, F.: Studies on clathrasils. VIII. Nonasils-$[4^15^8]$, $88\,SiO_2 \cdot 8\,M^8 \cdot 8\,M^9 \cdot 4\,M^{20}$: Synthesis, thermal properties, and crystal structure. J. Inclusion Phenom. **4** (1986) 339–349.

Mellini, M.; Merlino, St.: The crystal structure of jagoite. Amer. Mineral. **66** (1981) 852–858.

Penna, G.; Giese, Jr., R. F.: The crystal structure of wickenburgite, $Pb_3CaAl_2Si_{10}O_{24}(OH)_6$. Geol. Soc. Amer. Progr., Abstracts (1968) 232–233.

Pouchou, J. L.; Pichoir, F.: A new model for quantitative X-ray microanalyses. Part I: Application to the analysis of homogeneous samples. La Recherche Aerospatiale **3** (1984) 12–36.

Peiser, H. S.; Rooksby, H. P.; Wilson, A. J. C.: X-ray diffraction by polycrystalline materials. Chapman & Hall, London, (1960) pp. 392–393.

Sheldrick, G. M.: SHELXS-86. Program for crystal structure determination. University of Göttingen, Germany (1986).

Sheldrick, G. M.: SHELXL-93. Program for the refinement of crystal structure. University of Göttingen, Germany (1993).

Smith, D. K.; Roberts, A. C.; Bayliss, P.; Liebau, F.: A systematic approach to general and structure-type formulas for minerals and other inorganic phases. Amer. Mineral. **83** (1998) 126–132.

Spek, A. L.: PLATON, an integrated tool for the analysis of the results of single crystal structure determination. Acta Crystallogr. A46 (1990) C-34.

Williams, S. A.: Wickenburgite, a new mineral from Arizona. Amer. Mineral. **53** (1968) 1433–1438.